

PETO Interacts with Other Effectors of Cyclic Electron Flow in *Chlamydomonas*

Hiroko Takahashi^{1,4}, Stefan Schmollinger^{2,5}, Jae-Hyeok Lee³, Michael Schroda², Fabrice Rappaport¹, Francis-André Wollman¹ and Olivier Vallon^{1,*}

¹Institut de Biologie Physico-Chimique, UMR 7141 CNRS-UPMC, 13 rue P et M Curie, Paris 75005, France

²Molecular Biotechnology and Systems Biology, University of Kaiserslautern, Kaiserslautern 67663, Germany

³Department of Botany, University of British Columbia, Vancouver, BC V6T1Z4, Canada

⁴Present address: Graduate School of Science and Engineering, Saitama University, 255 Shimo-Okubo, Sakura-ku, Saitama 33808570 Japan

⁵Present address: Department of Chemistry and Biochemistry, University of California, Los Angeles, CA 90095, USA

*Correspondence: Olivier Vallon (ovallon@ibpc.fr)

<http://dx.doi.org/10.1016/j.molp.2015.12.017>

Note: This paper is dedicated to the memory of Fabrice Rappaport, who departed prematurely January 12, 2016

ABSTRACT

While photosynthetic linear electron flow produces both ATP and NADPH, cyclic electron flow (CEF) around photosystem I (PSI) and cytochrome *b₆f* generates only ATP. CEF is thus essential to balance the supply of ATP and NADPH for carbon fixation; however, it remains unclear how the system tunes the relative levels of linear and cyclic flow. Here, we show that PETO, a transmembrane thylakoid phosphoprotein specific of green algae, contributes to the stimulation of CEF when cells are placed in anoxia. In oxic conditions, PETO co-fractionates with other thylakoid proteins involved in CEF (ANR1, PGRL1, FNR). In *PETO*-knock-down strains, interactions between these CEF proteins are affected. Anoxia triggers a reorganization of the membrane, so that a subpopulation of PSI and cytochrome *b₆f* now co-fractionates with the CEF effectors in sucrose gradients. The absence of *PETO* impairs this reorganization. Affinity purification identifies ANR1 as a major interactant of PETO. ANR1 contains two ANR domains, which are also found in the N-terminal region of NdhS, the ferredoxin-binding subunit of the plant ferredoxin-plastoquinone oxidoreductase (NDH). We propose that the ANR domain was co-opted by two unrelated CEF systems (PGR and NDH), possibly as a sensor of the redox state of the membrane.

Key words: time-resolved spectroscopy, chlorophyll fluorescence, tridecyl-maltoside, sucrose gradient ultracentrifugation, state transition, STT7

Takahashi H., Schmollinger S., Lee J.-H., Schroda M., Rappaport F., Wollman F.-A., and Vallon O. (2016). PETO Interacts with Other Effectors of Cyclic Electron Flow in *Chlamydomonas*. *Mol. Plant*. **9**, 558–568.

INTRODUCTION

In oxygenic photosynthesis, linear electron flow (LEF) is driven by two photosystems, PSI and PSII, connected by the cytochrome *b₆f* (*cytb₆f*) complex embedded in the thylakoid membranes. This reaction produces ATP and NADPH at a theoretical ratio of 2.7:2, but ATP and NADPH are required at a ratio of 3:2 to sustain assimilation of CO₂ in the Calvin-Benson-Bassham cycle. Thus, extra ATP is needed for CO₂ fixation in the chloroplast. Import of ATP produced in the mitochondrion by oxidative phosphorylation or in the cytosol by glycolysis may fulfill this requirement, but additional photosynthetic sources of ATP can also be found in the chloroplast itself (Alic, 2010; Johnson, 2011). Pseudo-cyclic electron flow (“water-to-water cycles”) from water to molecular oxygen either through plastid terminal oxidase (Nawrocki et al., 2015) or direct O₂ reduction by PSI, the Mehler reaction (Miyake, 2010), can generate a proton gradient across

the thylakoid and thus drive ATP production by the ATP synthase. Cyclic electron flow (CEF) around PSI and *cytb₆f*, while also unable to produce reducing equivalents, uses the Q-cycle to pump protons into the lumen and is thus more energetically effective. In higher plants, two pathways have been distinguished for CEF, based on the site at which reducing equivalents generated by PSI photochemistry are re-injected into the membrane (Shikanai, 2007, 2014). One of them uses an NADH dehydrogenase-like (NDH) complex, accepting electrons from ferredoxin and reducing plastoquinone (PQ) in an electrogenic reaction (Shikanai et al., 1998; Ifuku et al., 2011; Yamamoto et al., 2011). Another pathway, antimycin A-sensitive in most organisms, is dependent on a

protein complex formed by PGR5, Proton Gradient Regulation 5 (Munekage et al., 2002) and PGRL1, PGR5-Like Photosynthetic Phenotype 1 (DalCorso et al., 2008). We refer to this hereafter as the PGR pathway. A double mutant lacking both the NDH and PGR pathways shows a severe growth phenotype in *Arabidopsis* (Munekage et al., 2004).

The green alga *Chlamydomonas reinhardtii* is a prominent microbial model in photosynthesis, and its photosynthetic apparatus is highly similar to that of land plants. In addition, it presents a highly diverse anaerobic metabolism allowing its survival in anoxic conditions via fermentation or hydrogen production (Hemschemeier and Happe, 2011; Catalanotti et al., 2013). In *Chlamydomonas*, two CEF pathways were also identified. Instead of the NDH complex, a single subunit NAD(P)H dehydrogenase (NDA2), which is similar to the yeast mitochondrial enzyme, allows reduction of the plastoquinone pool by NAD(P)H (Jans et al., 2008; Desplats et al., 2009). In addition, a PGR pathway has been described that is believed to represent a major supply of ATP for the cell (Tolleter et al., 2011; Johnson et al., 2014). In addition to PGR5 and PGRL1, Calcium Sensor (CAS; Petroustos et al., 2011) and Anaerobiosis Response 1 (ANR1; Terashima et al., 2012) have also been reported to contribute to the PGR pathway in *Chlamydomonas*. Cells placed in anoxic conditions display an increase in the rate of CEF, which has been attributed to the activation of the PGR pathway (Tolleter et al., 2011; Terashima et al., 2012; Alric, 2014; Johnson et al., 2014). These observations are in line with our original hypothesis that physiological conditions leading to State 2 were a prerequisite for establishment of a sustained CEF (Vallon et al., 1991; Majeran et al., 2001). In State 2, anoxia-induced over-reduction of the intersystem electron carriers activates the STT7 kinase that phosphorylates light-harvesting antenna proteins, triggering their movement to the unstacked membrane regions and their association with PSI (for reviews see Wollman, 2001; Rochaix, 2014). The activation of CEF in anoxia has even been proposed to be the result of a transition to State 2 (Finazzi et al., 2002). However, a comparison of wild-type and mutant lines locked in either State 1 or State 2 led us to conclude that the rate of CEF does not depend upon the reversible activation of the STT7 kinase but merely on the redox changes that develop between State-1 and State-2 conditions (Takahashi et al., 2013). In anoxia, the supramolecular organization of the thylakoid membrane also changes extensively. Immunogold labeling studies showed that a large fraction of *cytb₆f* moves from stacked to unstacked regions of the thylakoid membrane, along with light-harvesting complex II (LHCII) (Vallon et al., 1991), in an STT7 kinase-dependent process (Fleischmann et al., 1999). More recently, evidence has been gathered for a tight association between PSI and *cytb₆f* in *Chlamydomonas* cells kept in anoxia. A CEF supercomplex has been identified by sucrose density gradient fractionation of n-tridecyl-β-D-maltopyranoside (TDM)-solubilized thylakoids isolated from cells placed in State 2 by uncoupler treatment (Iwai et al., 2010). This fraction contained PSI, the major and minor LHCII antenna, *cytb₆f*, ferredoxin-NADP⁺ oxidoreductase (FNR) and PGRL1, all of which could be pulled down together using His-tagged PsaA. A CEF complex was also observed using n-dodecyl β-D-maltoside-solubilized thylakoids from anoxic cells (Terashima et al., 2012), with ANR1 co-migrating in the same region of the sucrose gradients. In our previous experiments using anoxic

cells, we observed a high molecular weight (MW) green band upon sucrose gradient centrifugation of TDM-solubilized membranes, whose detection correlated with the activation of CEF, being dependent on the redox status of the samples but not on the activation of the STT7 kinase (Takahashi et al., 2013).

In their mass spectrometry analysis of the gradient fractions containing the CEF supercomplex, Iwai et al. (2010) identified PETO, a nuclear-encoded thylakoid membrane protein (Hamel et al., 2000). This protein originally was described as a subunit of *cytb₆f* in *Chlamydomonas*, based on its deficiency in mutants lacking this protein complex, and therefore termed “subunit V” (Lemaire et al., 1986). PETO is a bitopic membrane protein exposing its C terminus to the stroma where it is reversibly phosphorylated during state transitions (Hamel et al., 2000). Later studies failed to identify PETO among the core subunits of the purified *b₆f* complex (Stroebel et al., 2003). Recently, we immunodetected PETO in a high-MW green band formed in anoxia (Takahashi et al., 2013). Interestingly, even in conditions where the CEF complex was not formed, we found PETO in high-MW fractions that also contained FNR and PGRL1 but not PSI or *cytb₆f*. This prompted us to further investigate the role of PETO in state transitions, in the formation of the CEF supercomplex and in the increased rates of CEF under anoxia. Here, we describe PETO-knockdown and -overexpression strains, and identify ANR1 as a major PETO interactant. Our results show that PETO contributes to the increase in CEF rate in anoxia and the stability of CEF supercomplexes, in conjunction with ANR1 and PGRL1.

RESULTS

Sequence Analysis of PETO

Our previous study (Hamel et al., 2000) identified the PETO gene in *Chlamydomonas*, but no homolog could subsequently be identified in the genome of vascular plants. Extensive mining of sequence data from microalgae allowed us to identify PETO orthologs exclusively in chlorophytes (green algae) belonging to the clades Chlorophyceae and Trebouxiophyceae, but not in Prasinophyceae, the most ancestral clade (alignment in Supplemental Figure 1). In all these sequences, a bipartite chloroplast transit peptide targets the protein to the thylakoid, placing the mature N terminus in the lumen, while a conserved transmembrane helix places the C terminus on the stromal surface. On average, mature PETO has a MW of 15.4 kDa and a basic *pI* (9.64), due to the presence of many lysine residues (see Supplemental Table 1). Its high lysine content may explain why the *Chlamydomonas* protein stains very well with Coomassie blue (Lemaire et al., 1986). The C-terminal domain shows a conserved (K/R) (D/N)SX₄₋₅G(Y/F)E motif, but the strictly conserved Ser is not among the nine residues recently found to be phosphorylated in PETO (Bergner et al., 2015). PETO ends with a poorly conserved region that is very basic (*pI* = 10.8) and enriched in lysine and glycine residues (respectively 19.5% and 15.0% in *C. reinhardtii* PETO, versus 2.4% and 11.4% in the entire proteome).

Characterization of Strains Underexpressing or Overexpressing PETO

To gain further insight into the function of PETO, we generated PETO underexpressing and overexpressing strains in

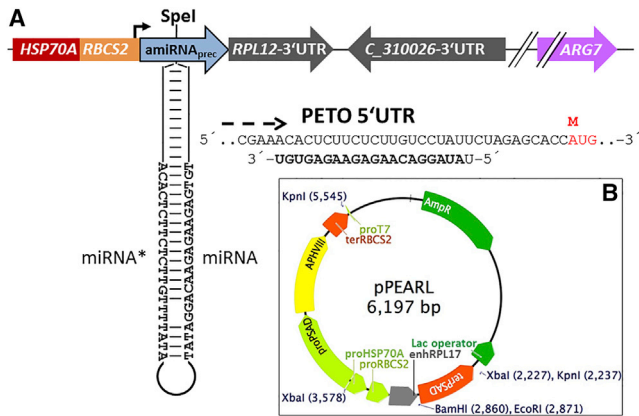


Figure 1. Constructs for PETO Knockdown and Overexpression.

(A) Artificial microRNA in plasmid pChlamiRNA2 (features not to scale) and target in PETO (sequence corresponds to Cre12.g558900.t1.2 gene model, but transcription actually starts upstream).

(B) pPEARL vector (CDS of transgene is introduced between the *Bam*HI and *Eco*RI sites).

C. reinhardtii. Knockdown of PETO was achieved utilizing a constitutively expressed artificial microRNA (amiRNA) (Molnar et al., 2009), targeting a sequence in the 5' untranslated region (UTR) of the gene (Figure 1A). Of 74 transformants screened by western blotting, 18 were found to have a reduced content in PETO. Four of these knockdown strains (PETO-KD) were retained that had PETO levels below 5% of that in control strains (WT-C), i.e. strains obtained by transformation of the recipient strain with the empty vector (Figure 2A). To overexpress PETO, we used the newly designed vector pPEARL (Figure 1B), where the CDS of the protein to be expressed is placed downstream of the ARL control element. This module is derived from the efficient *HSP70A-RBCS2* tandem promoter (Schroda et al., 2002) by adding an enhancer originating from the first intron of the *RPL17* gene coding for a large ribosome subunit. This modification leads to increased robustness of transgene expression compared with the *HSP70A-RBCS2* promoter alone (Joo and Lee, unpublished data). The plasmid also contains an *APHVIII* selection marker (Sizova et al., 2001), allowing selection of transformants on paromomycin. Two versions of the PETO plasmid were constructed, without or with a C-terminal Strep-tagII, to allow purification by affinity. Since the amiRNA used to down-regulate PETO targets the 5' UTR, it is not expected to hamper expression of the PETO transgene. We were therefore able to transform the PETO overexpression constructs into a PETO-KD strain so that all PETO is tagged. We selected PETO-overexpression strains carrying the Strep-tagII (PETO-OS) or not (PETO-OE) (Figure 2B). The PETO accumulation level in these strains was more than two-fold that in control strains (Figure 2C).

PETO-KD, PETO-OE, and PETO-OS grew photo-autotrophically with no evidence for increased light sensitivity or inability to utilize intermittent light. This is shown for several PETO-KD transformants in Supplemental Figure 2. Chlorophyll fluorescence induction curves were qualitatively similar to those of control strains (not shown), as was variable chlorophyll fluorescence Fv/Fm (Table 1) and the dependency of Φ_{PSII} on light intensity

(Supplemental Figure 3). Key PSI and PSII subunits as well as proteins involved in CEF and chlororespiration accumulated at levels similar to those in the control (Figure 3A). In particular, we noted that cytochrome *f* accumulation in PETO-KD (Figure 2A) and PETO-OE (Figure 2C) was commensurate with that in wild-type strains.

We then investigated PETO protein contents in several photosynthesis mutants compromised in the activity of distinct thylakoid membrane proteins. As shown previously (Lemaire et al., 1986; Hamel et al., 2000), PETO accumulation was dramatically decreased in mutants lacking the *cytb₆f* complex (e.g. Δ *petA* in Figure 3B). In contrast, PETO levels remained wild-type-like in mutants assembling an enzymatically inactive *cytb₆f* complex. This is exemplified in Figure 3B by the *PETC-Δ1* mutant, where a *cytb₆f* complex lacking the Rieske protein accumulates in exponentially growing cells (de Vitry et al., 1999), as well as in the *petD-PEWY* mutant that lacks *cytb₆f* activity due to an alteration of the *Q_o* site (Zito et al., 1999). All of the other mutants we investigated, lacking either PSI, PSII, plastocyanin, PTOX2, NDA2, PGR5, or PGRL1, accumulated PETO at wild-type levels (Figure 3B).

When investigating the PETO content under various environmental conditions, we observed no changes in PETO protein accumulation when cells were incubated for 4 or 24 h in anoxic conditions (Figure 4A and 4B). At the mRNA level, a slight decrease was observed during dark anoxic treatment, as judged by examination of experiment GSE42035 on the *Chlamydomonas* genome browser (<http://phytozome.jgi.doe.gov>; see also Supplemental Table 1). Interestingly, we noted some increase in cytochrome *f* accumulation upon prolonged incubation in anoxia (Figure 4B). This was true for the control as well as for a PETO-KD strain, ruling out a role for PETO in this response. A modest induction of the ANR1 protein could also be observed in anoxia (Figure 4A), in line with previous observations (Terashima et al., 2010). Interestingly, the ANR1 protein level was lower in the PETO-OE strains, a result confirmed in the PETO-OS strain (not shown). We also compared mixotrophic with photo-autotrophic cultures, i.e. cells grown in the light with or without acetate in the medium (Figure 4C and 4D). We found that PETO protein levels were about 1.8-fold higher in the latter condition, on a chlorophyll basis as well as relative to the content in β -CF1.

Because earlier studies suggested a possible involvement of the PETO phosphoprotein in state transitions (Hamel et al., 2000), we assessed the efficiency of this regulation in PETO-OE and PETO-KD strains. To this end, we monitored changes in the maximal fluorescence level (Fm), an indirect measure of the fraction of light-harvesting antenna associated with PSII. After placing the cells in State 2 by anoxia, we measured the amplitude and kinetic parameters of the transition from State 2 to State 1 during illumination in the presence of 3-(3,4-dichlorophenyl)-1,1-dimethylurea (DCMU), and back to State 2 when cells were returned to darkness (Table 1). No differences were observed between PETO-KD, PETO-OE, and WT-C strains, neither in the kinetics nor in the amplitude of state transitions. We also observed that the phosphorylation pattern of antenna proteins during transition from State 1 to State 2 was not affected in PETO-KD (Supplemental Figure 4). We thus found no evidence

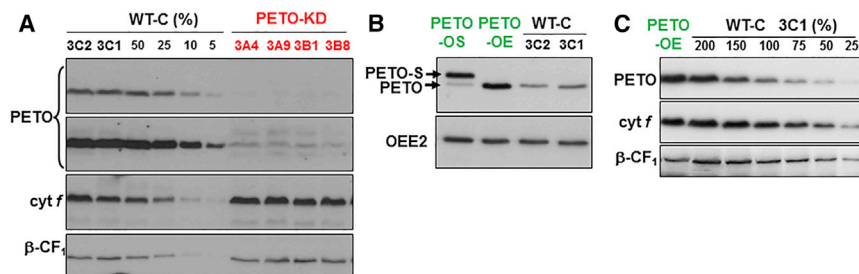


Figure 2. Characterization of PETO-KD, -OE, and -OS Strains.

(A–C) Immunoblots of total cellular extracts (1 μg of chlorophyll corresponding to 100% and serial dilutions for the WT-C), using antisera against PETO, cytf, β-CF₁, and OEE2 (as loading controls). In (A), a short and a long exposure are shown for PETO.

for any critical contribution of PETO to the reorganization of the light-harvesting antenna during state transitions in *Chlamydomonas*.

PETO Is Part of a High-MW Complex that Shifts Size and Composition during Anoxia

To identify proteins interacting with PETO, we subjected thylakoid membranes to mild detergent solubilization using TDM, followed by sucrose gradient centrifugation as described earlier (Takahashi et al., 2013). Preliminary experiments revealed that PETO was found in heavy fractions even at a high detergent concentration of 1% (Supplemental Figure 5) where its distribution showed no overlap with that of PSI, PSII, or cytb₆f, all found in lighter fractions. In subsequent studies, we chose a TDM concentration of 0.85% as optimal for the separation of green bands corresponding to PSI, PSII, and LHCII. Figure 5A presents the immunodetection of PETO and other proteins of interest in gradients obtained with thylakoids derived from normoxic cells (aerobically grown and pre-illuminated in the presence of DCMU to fully oxidize the PQ pool). In the control strain, PETO was found to migrate in fractions 5–11 with a peak in fraction 9, i.e. lower than the major cytb₆f and PSI fractions (respectively in fractions 12–19 and 9–15). Interestingly, ANR1 had a distribution very similar to that of PETO, as did FNR. PGRL1 had a bimodal distribution with the heavier population co-migrating with PETO. Evidence that these co-fractionation patterns were likely to reflect genuine protein–protein interactions came from the analysis of the PETO-KD strain: the distribution of FNR and PGRL1 now drifted toward lighter fractions (respectively 9–12 and 7–16). The distribution of ANR1 broadened significantly, although the bulk of the protein remained in heavy fractions. The small amount of PETO remaining in the PETO-KD extract was found at the same position as in the control (arrowhead in Figure 5A). These results suggest that PETO, ANR1, FNR, and a fraction of PGRL1 are part of a high-MW complex, or at least

that they reside in a membrane microdomain that resists TDM solubilization. It should be noted that in the absence of PETO ANR1 still migrated in heavy fractions, far below what is expected from its small MW, indicating that it either forms oligomeric structures or remains in a detergent-resistant membrane domain.

As previously reported by Takahashi et al. (2013), subjecting the cells to anoxia changed the fractionation pattern in the gradient with, in particular, an increased amount of material migrating in the high-MW region (Figure 5B). We note, however, that the contrast between normoxic and anoxic conditions was less clear cut than previously observed. Comparison of the gradients obtained in these two conditions with the WT-C, PETO-KD, and PETO-OE strains revealed possible roles of PETO in this reorganization. In the WT-C and PETO-OE strains, the fraction of cytb₆f co-migrating with PSI was larger in anoxic conditions, as previously shown, even if the shift was less pronounced than in our previous report. This change was less marked in the PETO-KD strain. Anoxia also led to changes in the distribution of FNR, PGRL1, ANR1, and PETO, with a large fraction of these proteins now co-migrating with PSI. Here again, the PETO-KD strain behaved differently from the other two, with a broader distribution of FNR, ANR1, and PGRL1, all shifting toward lighter fractions. Taken together, these observations suggest that in the absence of PETO, the interactions between other CEF effectors, PSI, and cytb₆f in anoxic conditions are weakened.

Probing the Interactions of PETO with Proteins Involved in CEF

In an attempt to understand whether co-migration of PETO with CEF complex components reflected genuine molecular interactions, we developed an affinity purification strategy using Strep-tagged PETO (PETO-OS) as bait (Figure 6). TDM-solubilized membranes from PETO-OS strain were loaded onto a streptactin

Photosystem II		State transitions		
	Fv/Fm	(Fm1 – Fm2)/Fm1 (%)	t _{1/2} (min) State 2 to 1	t _{1/2} (min) State 1 to 2
WT-C	0.69 ± 0.04	19 ± 4	6.9 ± 1.5	3.4 ± 0.9
PETO-KD	0.69 ± 0.03	22 ± 7	6.1 ± 1.5	3.5 ± 0.6
PETO-OE/OS	0.71 ± 0.03	21 ± 3	6.2 ± 0.7	5.1 ± 1.8

Table 1. Changing PETO Level Does Not Affect PSII Activity or State Transitions.

Fv/Fm and amplitude and half-time of transition from State 2 to State 1 and back to State 2 in WT, PETO-KD, and PETO-OE. Four strains were used for WT-C and PETO-KD, one each for PETO-OS and PETO-OE. For Fv/Fm, values are the average and SD of eight measurements per strain. For state transitions, four measurements per strain were taken for WT-C and PETO-KD, and three for PETO-OS and PETO-OE. Amplitude of state transitions is lower than in previous reports (Wollman and Delepelaipe, 1984), probably due to the 96-well plate setup.

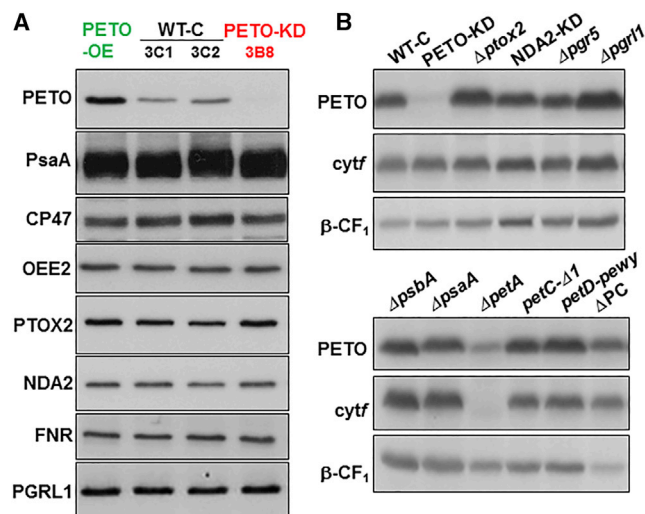


Figure 3. Immunoblot Analysis of Photosynthetic Proteins in PETO and CEF/LEF Mutants.

Accumulation of proteins involved in LEF, CEF, or chlororespiration in PETO mutants (A) and PETO accumulation in various photosynthesis mutants (B). Total cellular extracts (1 μ g of chlorophyll) from control (WT-C), PETO mutants, and photosynthesis mutants were assayed by immunoblotting using antisera against various thylakoid membrane proteins.

column, washed, and eluted with desthiobiotin, which competes with the Strep-tagII peptide for interaction with the column. The fractions were characterized by immunoblotting. Comparison of the input (In), the unbound flow-through (Ub), and the fraction collected after the first washing step (W1) shows that almost all of the tagged PETO was retained on the column. Elution released PETO along with a small fraction of ANR1 and even smaller amounts (compared with the immunoreactivity in the input) of PGRL1. Traces of PsaA and FNR were also observed, but none of cytochrome *f*. OEE2 (PSII) and β -CF₁ (ATPase) also were not retained on the column. This experiment thus reveals a specific interaction of PETO with ANR1. Interactions, direct or indirect, with other components of the CEF complex cannot be ruled out, but are not robust enough to be preserved in our experimental conditions.

PETO Is Involved in the Rapid Switch from LEF to CEF in Anoxic Conditions

Because the results above suggested an interaction of PETO with the other effectors of CEF, we set out to determine how its quasi-absence in PETO-KD affects CEF rates. At the onset of anoxia, P700 photo-oxidation cannot be measured because of rapid back-reaction between P700⁺ and the Fe-S centers, due to PSI acceptor side limitation. As we showed previously, this “blocked state” is eventually relieved during incubation in the dark through the activation of an anaerobic metabolism that results in the reoxidation of ferredoxin and PSI acceptors (Takahashi et al., 2013; Clowez et al., 2015). Unfortunately, the rate of unblocking was found to vary greatly between different genetic backgrounds, and the protocol used in Takahashi et al. (2013) could not be applied here. However, we recently showed (Clowez et al., 2015) that a continuous illumination of anoxic samples in the presence of DCMU stimulates ATP-dependent NADPH

oxidation reactions and thus leads to the rapid alleviation of PSI acceptor side limitation. Under actinic illumination (115 μ mol photons $m^{-2} s^{-1}$), PSI unblocking in WT-C, PETO-KD, and PETO-OE strains was achieved in 60 s, with similar kinetics (Supplemental Figure 6). We noticed that 10%–15% of the original P700 signal could not be recovered by illumination of anoxic cells (Supplemental Figure 6), but the presence of a small fraction of blocked PSI centers does not significantly affect our measurements of CEF rates. Our protocol thus allows us to measure the P700 photo-oxidation level both in normoxia and anoxia, using a 120-s pre-illumination period (Supplemental Figure 7). In these experiments, the difference between steady-state and maximal (pulse-induced) P700 photo-oxidation reflects CEF. As expected, the P700 photo-reduction activity was largely sensitive to DBMIB, an inhibitor of the Q_o site of *cytb₆f* (Supplemental Figure 8A). Under oxic conditions, the drug leads to an almost complete photo-oxidation of P700, even if some reducing activity remains. When added to anoxic cells, DBMIB instantaneously restores 90%–98% of the initial P700 maximum photo-oxidation. This is consistent with the results of Clowez et al. (2015), who have shown that a mutant in *cytb₆f* fails to undergo PSI acceptor side limitation in anoxia because not enough electron donors are available to reduce the primary acceptors. In DBMIB-treated anoxic cells, the level of steady-state P700 photo-oxidation under illumination of 115 μ mol photons $m^{-2} s^{-1}$ was 4%–6% below the maximum level induced by the pulse, consistent with a low residual level of electron transfer to P700. A similar level of residual activity was found by Clowez et al. (2015) in *cytb₆f* and plastocyanin mutants. Here, the DBMIB-insensitive activity was similar between the three genotypes (Supplemental Figure 8B). Finally, note that the P700 photo-oxidation activity depends on the PSI antenna size. Based on ECS measurements, it varied by less than 13% between our strains in normoxia (State 1) and increased in anoxia (State 2) by 38%, 33%, and 31% for WT-C, PETO-KD, and PETO-OE, respectively. Because our calculations normalize CEF rates to the activity of PSI charge separation, they will not be affected by these small differences in PSI antenna size.

Based on the considerations above, we consider that the steady-state level of P700 photo-oxidation in DCMU-poisoned cells represents a reliable basis for CEF in our strains. As shown in Figure 7, the CEF rates in normoxia were similar between the three genotypes (*t*-test *p* value: WT/OE, 0.36; WT/KD, 0.70). In anoxia, rates increased significantly in WT-C and PETO-OE compared with normoxia (1.9-fold and 2.4-fold, *p* = 0.005 and *p* = 0.013, respectively). The two genotypes can be considered as behaving similarly in anoxia (*p* = 0.76). The observed increase is in the same range as we previously reported with other strains measured in dark-adapted samples (Takahashi et al., 2013). In PETO-KD strains, however, the rate obtained in anoxia was significantly lower than in the wild-type (*p* = 0.012). Moreover, the increase caused in PETO-KD strains by anoxia, compared with normoxia, cannot be considered as highly significant (*p* = 0.032). We conclude that PETO is essential for the stimulation of CEF when *Chlamydomonas* cells are placed in anoxia.

Based on the considerations above, we consider that the steady-state level of P700 photo-oxidation in DCMU-poisoned cells represents a reliable basis for CEF in our strains. As shown in Figure 7, the CEF rates in normoxia were similar between the three genotypes (*t*-test *p* value: WT/OE, 0.36; WT/KD, 0.70). In anoxia, rates increased significantly in WT-C and PETO-OE compared with normoxia (1.9-fold and 2.4-fold, *p* = 0.005 and *p* = 0.013, respectively). The two genotypes can be considered as behaving similarly in anoxia (*p* = 0.76). The observed increase is in the same range as we previously reported with other strains measured in dark-adapted samples (Takahashi et al., 2013). In PETO-KD strains, however, the rate obtained in anoxia was significantly lower than in the wild-type (*p* = 0.012). Moreover, the increase caused in PETO-KD strains by anoxia, compared with normoxia, cannot be considered as highly significant (*p* = 0.032). We conclude that PETO is essential for the stimulation of CEF when *Chlamydomonas* cells are placed in anoxia.

DISCUSSION

In this study, we show that absence or overexpression of *PETO* has no effect on the accumulation level of the *cytb₆f* complex.

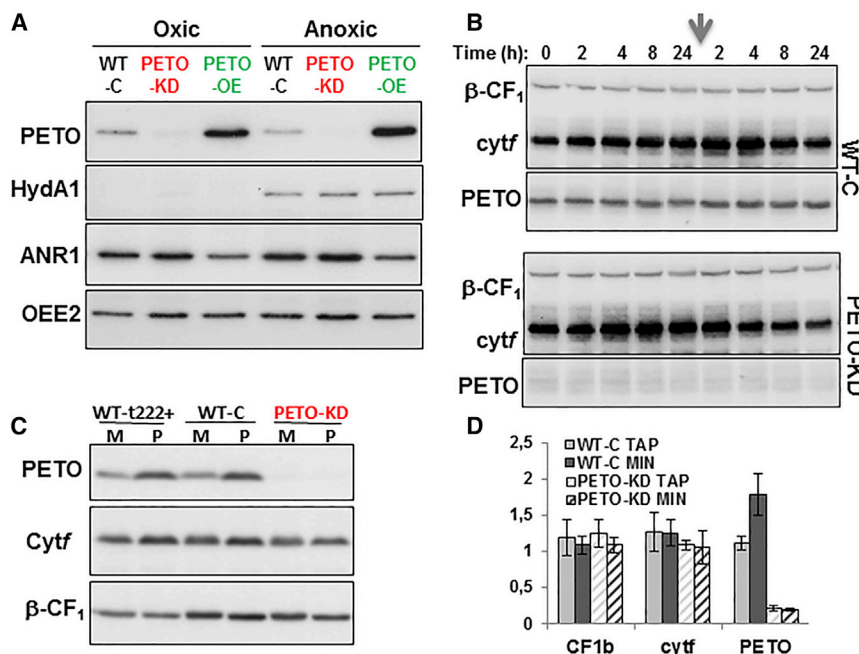


Figure 4. Changes in PETO Levels in Various Conditions.

Anaerobiosis was obtained by bubbling argon for 4 h (A) or nitrogen for 24 h before return to air as shown by arrow (B). Mixotrophic versus photoautotrophic growth (C and D). Total cellular extracts (1 μg of chlorophyll) were assayed by immunoblotting, OEE2 and β-CF₁ being used as loading controls. In (A), efficacy of anoxic treatment is attested by the induction of the HydA1 hydrogenase. In (C), M indicates mixotrophic, and P photo-autotrophic conditions. In (D) quantification (±SD) of immunochemical signal for β-CF₁, cytf, and PETO was averaged over three WT-C and four PETO-KD biological replicates. Data are normalized to the value in WT strain WT-t222+ grown in TAP.

(Takahashi et al., 2013; Bergner et al., 2015). We note that Bergner et al. (2015), using a solubilization procedure different from ours, found that absence of STT7 shifts PETO to lighter fractions in their sucrose gradients, suggesting that its phosphorylation strengthens interactions with other proteins in the membrane.

Yet the fact that PETO accumulation selectively depends on the presence of *cytb₆f* suggests some form of interaction, even if our affinity purification experiments, performed in anoxia, could not demonstrate it. Interestingly, mutants with inactive or defective *cytb₆f* complexes accumulate PETO normally, which indirectly shows that PETO accumulation does not depend on the activation of the STT7 kinase that requires *cytb₆f* activity. It is also worth noting that the PETO protein rapidly disappears during nitrogen starvation along with the *cytb₆f* subunits, while at the same time the chlororespiratory enzymes PTOX2 and NDA2 overaccumulate (Wei et al., 2014). Expression of the *PETO* gene also is shut down in these conditions, as revealed by analysis of experiment GSE34585 (Supplemental Table 1). Because the disappearance of PETO is rapid, preceding even that of *cytb₆f* subunits, these findings suggest that the PETO protein turns over rapidly, at least during nitrogen starvation. Decreased *PETO* transcripts have also been observed under strong Fe deficiency (GSE35305) and to a lesser extent during prolonged anaerobiosis (GSE42035). Finally, we found that accumulation of the protein was increased in photo-autotrophically grown cells (Figure 4). This could reflect a higher requirement for CEF in these conditions, when the extra ATP needed for CO₂ fixation cannot come from the respiration of exogenous carbon sources.

Changing the PETO level did not affect the amplitude or kinetics of state transitions (Table 1), nor the phosphorylation pattern of antenna proteins (Supplemental Figure 4). This result was rather unexpected, as phosphorylation of PETO has been demonstrated by *in vivo* ³²P labeling to be dynamic and to increase State-2 conditions (Hamel et al., 2000). A recent phosphoproteomic study of thylakoid membranes (Bergner et al., 2015) showed that phosphorylation of PETO is higher in anoxic compared with high light conditions, and depends on the state transition kinase STT7. However, STT7-dependent PETO phosphorylation is certainly not necessary for stimulation of CEF, since this response is also observed in *stt7* mutants

phosphorylation strengthens interactions with other proteins in the membrane.

Most importantly, our analysis of CEF rates shows that PETO is essential for the stimulation of CEF when *Chlamydomonas* cells are placed in anoxia (Figure 7). The small anoxia-induced increase in CEF rate measured in PETO-KD strains cannot in fact be considered as significant. Mutants in PGRL1, PGR5, ANR1, and CAS have also been shown to be affected in the stimulation of CEF in anoxic *Chlamydomonas* cells (Tollete et al., 2011; Terashima et al., 2012; Johnson et al., 2014), so PETO can now be added to this already long list. Rates of CEF in anoxia thus appear to be determined not only by the redox poise of the chloroplast stroma and membrane components, but also by a host of effector proteins that modulate its efficiency. Mutations in the CEF effectors PGRL1, PGR5, and ANR1 result in increased PSI light sensitivity, a phenotype exacerbated in the case of the *pgr1* mutant by the absence of LHCSR3-dependent qE (Terashima et al., 2012; Johnson et al., 2014; Bergner et al., 2015). Such a PSI photosensitivity was not observed in our experiments, probably due to the fact that the effect of PETO on CEF is observed only in anoxia, where PSI is protected from photo-damage.

A possible clue about the mechanism by which PETO affects CEF came from the observation of interactions between PETO and ANR1. Genetic interaction is demonstrated by the observed decrease in ANR1 accumulation when PETO is overexpressed (Figure 4A). We also show that PETO co-migrates with ANR1 in sucrose gradients, already in oxic conditions (Figure 5). PGRL1 and FNR also peaked in the same fractions of the gradient, and the fact that PETO knockdown modified their distribution is strong evidence for some form of interaction, direct or indirect. Rather than a “complex” or “supercomplex,” which seem to imply a fixed stoichiometry of the constituents, we prefer to think of this object of very large and apparently heterogeneous

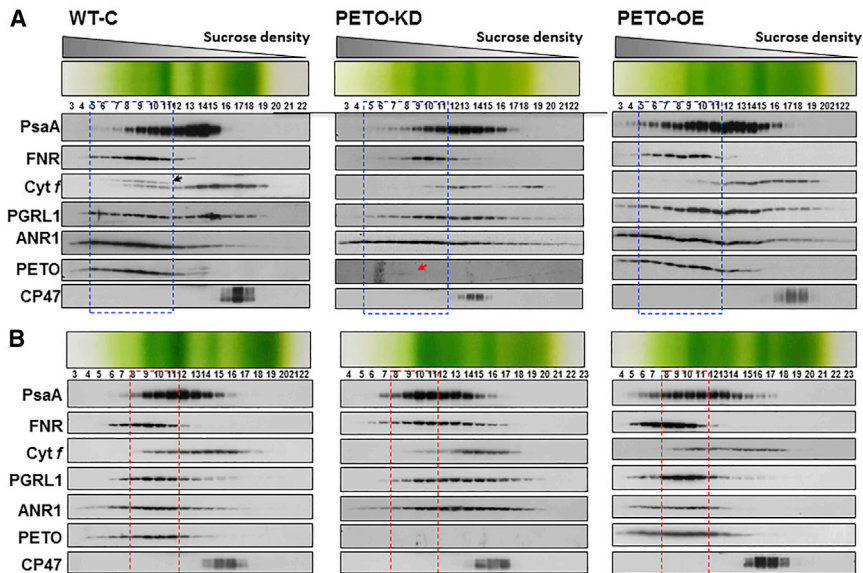


Figure 5. Sucrose Density Gradient Fractionation.

Thylakoid membranes were isolated from oxic (A) or anoxic (B) cells from WT-C (left), PETO-KD (center), and PETO-OE (right), solubilized with 0.85% TDM and fractionated by SDG ultracentrifugation. Gradient fractions were subjected to immunoblotting using antisera against PsaA, FNR, Cyt *f*, PGRL1, ANR1, PETO, and CP47. The red arrow indicates the trace amount of PETO in PETO-KD, and the black arrow in WT-C a nonspecific cross-reaction in this particular Cyt *f* blot. The dashed area covers the region of the gradient where the bulk of PETO migrates in oxic (blue) and anoxic (red) conditions in the WT-C strain.

size as a membrane microdomain, resistant to TDM solubilization, comprising PETO, ANR1, PGRL1, FNR, and possibly other constituents. Because ANR1 is the least affected of the CEF effectors when PETO is missing, it may be viewed as a core component of this microdomain. In anoxia, a reorganization of the membrane occurs that places CEF effectors in the same gradient fractions as a subpopulation of PSI and *cyt_bf*, which corresponds to the polypeptide profile of the CEF supercomplex previously described (Iwai et al., 2010; Terashima et al., 2012; Takahashi et al., 2013). Final evidence for an interaction between PETO and ANR1 came from Strep-tag affinity purification, where a sizable fraction of ANR1 was retained on the column and eluted along with PETO. Here also, interaction with PGRL1 and FNR could be documented, but involving a much smaller proportion of these proteins. This could mean that an indirect association exists but is too weak to resist the rather harsh procedure needed to wash the column. It must also be emphasized that the stoichiometry of all these CEF effectors is still unknown. In the absence of absolute protein quantification, mRNA levels remain the best proxy. By averaging normalized read counts over the 133 RNA-sequencing experiments displayed on the Phytozome browser (Supplemental Table 1), we found that the *PETO* mRNA level was about one-quarter that of *ANR1* and one-half that of *FNR*, but about two-fold larger than those of *PGRL1* and *PGR5*.

Based on the discussion above, ANR1 appears as a crucial player in the modulation of CEF. It is found in all chlorophyte algae (Supplemental Figure 9) and is thus more ancient than PETO. Note that the Chlorophyceae *Monoraphidium neglectum* and *Chlamydomonas euryale* contain two paralogs of both ANR1 and PETO, proof of two independent events of concerted duplication of these genes. Analysis of the ANR1 sequence reveals a few interesting properties. It is usually anchored to the membrane by three transmembrane helices, even if the main *C. reinhardtii* isoform has only one. Interestingly, Prasinophyceae of clade II (*Ostreococcus*, *Micromonas*, *Monomastix*) contain a paralog, which we call ANL1 for ANR1-Like, that lacks the transmembrane domain. The soluble domain

of ANR1 consists of a duplication of a 66-residue “ANR domain” containing a highly conserved “GGE motif” (see alignment in Supplemental Figure 9 and sequence logos in Figure 8). Interestingly, a similar duplicated domain has also been described at the N terminus of NdhS in vascular plants (Ifuku et al., 2011; Yamamoto et al., 2011). NdhS (initially named CRR31) is the ferredoxin-binding subunit of the chloroplastic ferredoxin-plastoquinone oxidoreductase, NDH (Yamamoto et al., 2011; Yamamoto and Shikanai, 2013). At the C terminus, it contains a hydrophilic SH3-like domain similar to PsaE, which binds ferredoxin. The N-terminal domain, where similarity to ANR1 can be found, appears dispensable for catalysis and its function remains elusive. The alignment of algal ANR1 proteins shown in Supplemental Figure 9 includes the second ANR domain of NdhS proteins found in those Prasinophyceae that have retained the NDH complex (Lemieux et al., 2014). The high sequence similarity leaves no doubt that ANR1 and NdhS are homologous. By comparison, the first ANR domain of NdhS is more divergent, as shown in the alignment of NdhS proteins (Supplemental Figure 10) and in the sequence logos of Figure 8, but the core of the GGE motif is still clearly recognizable. Interestingly, plants of the class Fabaceae also contain paralogous proteins that we propose to call CRL31 for CRR31-Like (Supplemental Figure 10), which lack the C-terminal SH3-like domain and thus resemble ANL1 proteins of algae. In *Arabidopsis*, NdhS forms a 300-kDa complex with NdhT and NdhU (Yamamoto et al., 2011), two DnaJ domain-containing proteins with a C-terminal TM-helix, but only NdhT is found in cyanobacteria and those Prasinophyceae that contain the NDH complex. Figure 9 summarizes our findings on the phyletic distribution of PETO, ANR1, NdhS, and related proteins in cyanobacteria, chlorophytes, and streptophytes.

What could be the function of the duplicated ANR domain? We would like to speculate here that this function is regulatory and related to redox sensing. Regulation of CEF by the redox state of the stroma has been attributed to PGRL1, which has six widely conserved cysteine residues of which two can be reduced by thioredoxin (Hertle et al., 2013). The activity of NDH also appears negatively regulated by thioredoxin (Courteille et al., 2013). However, additional regulatory mechanisms could be at play, for example at the level of the PQ redox state or the

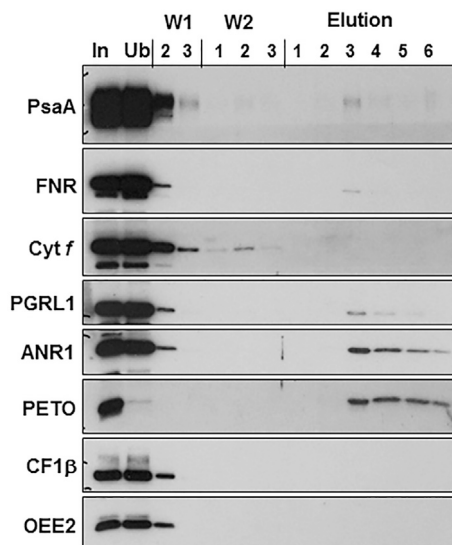


Figure 6. Strep-tagII Affinity Chromatography.

Thylakoid membranes from anoxic PETO-OS cells were solubilized with TDM and loaded onto a streptactin column. Gel loading corresponds to 0.3 μg of chlorophyll for input (In) and unbound (Ub) fractions, 1:100 volume for each wash fraction and 1:50 for each eluate fraction.

transmembrane proton gradient, either of which the ANR domain could sense thanks to its membrane association. In the case of NdhS, this could affect its affinity for the NDH complex and, thus, ferredoxin oxidoreductase activity. NDH activity usually contributes only a minor fraction of total CEF (Johnson, 2011), but it could function to alleviate stromal over-reduction under stress conditions (references in Ifuku et al., 2011) and/or to regulate the proton-motive force via ATPase activity (Wang et al., 2015). Disconnecting NdhS from the complex could prevent redox equilibration between ferredoxin and PQ in the dark, possibly affecting regulatory processes in the stroma. In the case of ANR1, activation of the ANR domain in anoxia could be transduced into a reorganization of the microdomain that sequesters ANR1, PETO, PGRL1, and FNR. This would in turn facilitate the formation of the CEF complex and allow interaction between FNR and *cytb₆f*, which in plants has been proposed to be necessary for the establishment of CEF (Joliet and Johnson, 2011). It remains to be determined whether this reorganization is connected to the STT7-dependent redistribution of *cytb₆f*, a large fraction of which moves from appressed to unappressed regions during transition to State 2 in anoxia (Vallon et al., 1991), (Fleischmann et al., 1999).

The origin of PETO is relatively recent in the evolution of chlorophytes, so its role could be as a secondary modulator of the ANR1-mediated regulation, possibly sensing the stromal redox state via its C-terminal domain. PETO obviously contributes to the stability of the ANR1/PGRL1/FNR microdomain in oxic conditions, and this in itself could affect the efficiency of CEF complex formation when the cells are placed in anoxia.

METHODS

Strains and Plasmids

The *C. reinhardtii* strain *arg7 mt* that was used as a recipient for transformation can be obtained from <http://chlamystation.free.fr/>. PETO knock-

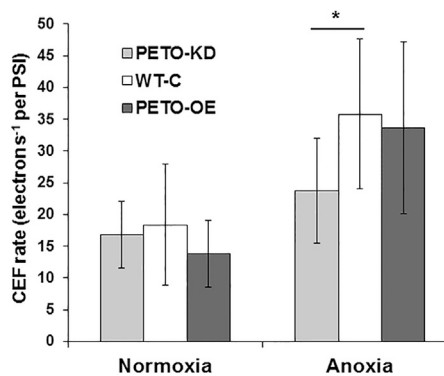


Figure 7. CEF Rates Measured in Oxic and Anoxic Conditions in PETO-KD, WT-C, and PETO-OE Strains.

Average (±SD) of nine measurements for WT-C (three independent strains), 12 for PETO-KD (four strains), and five for PETO-OE/OS. Asterisk indicates significant difference determined by Student's *t*-test, *p* < 0.02.

down strains were generated by artificial microRNA (amiRNA) interference, as described previously (Molnar et al., 2009; Schmollinger et al., 2010). The amiRNA target region within the *PETO* gene was identified with the help of the WMD2 tool (Ossowski et al., 2008) (<http://wmd3.weigelworld.org>). Resulting oligonucleotides *ctagtACACTCTTCTCTTGTTTATAtctcgctgcatcgccaccatgggggtgggtgatcagcctaTATAGGACAAGAGAAGAGTGTg* and *ctagcACACTCTTCTCTTGTCTATatagcgtgatcaccaccaccatggtgccgatcagcgagaTATAAAACAAGAGAAGAGTGTa* (uppercase letters indicating miRNA*/miRNA regions within the oligonucleotides) were annealed and cloned into pChlamiRNA2 (Molnar et al., 2009), yielding pMS589, where amiRNA expression is driven by the constitutively active, strong *HSP70A/RBCS2* tandem promoter (Schroda et al., 2002).

The overexpression vector pPEARL (paromomycin-resistant expression vector driven by ARL element, Figure 1B) was constructed by first combining in a pBS-SK+ plasmid an *EcoRI/KpnI* fragment, excised from pSI103 (Sizova et al., 2001), containing the *APHVIII* coding sequence and *RBCS2* terminator, with a PCR-generated *XbaI/EcoRI* fragment containing the *PSAD* promoter (Fischer and Rochaix, 2001). The hybrid ARL control element was engineered by combining in pBS-SK+ an *XbaI/BamHI* fragment of the *HSP70A-RBCS2* fusion promoter (Schroda et al., 2002) with a *BglII/EcoRI* PCR-amplified fragment of the *RPL17* gene (Cre13.g568900) coding for ribosomal protein L17. This fragment contains the first intron of the gene, but starts after the *RPL17* initiation codon and will thus constitute the 5' UTR of the transgene. A PCR-amplified fragment of the *PSAD* terminator (Fischer and Rochaix, 2001) flanked at 5' by *BamHI/EcoRI* and at 3' by *KpnI/XbaI* sites was added, then the whole element was ligated into the *XbaI*-digested *APHVIII* plasmid modified to eliminate *EcoRI/BamHI* sites. A plasmid with head-to-head oriented promoters was selected as pPEARL. To overexpress *PETO*, its entire CDS, PCR-amplified from cDNA introducing a Strep-tagII sequence (WSHPQFEK) at the C terminus, was cloned into pPEARL, using the unique *EcoRI* and *BamHI* sites between the ARL17 element and *PSAD* terminator. The resulting pHT1 plasmid was further modified by cutting with *BstZ17I* and *BamHI*, Klenow fill-in, and religation, yielding pHT2 where the Strep-tagII was removed. Both plasmids were transformed into PETO-KD strain 3B8.

Growth Conditions

Cells were grown to mid-log phase (3–5 × 10⁶ cells/ml) in Tris acetate-phosphate (TAP) medium at 25°C under 50 μmol photons m⁻² s⁻¹ or in mineral (MIN) medium at 100 μmol photons m⁻² s⁻¹. Total cellular proteins were extracted and assayed as described by Takahashi et al. (2013).

Molecular Plant

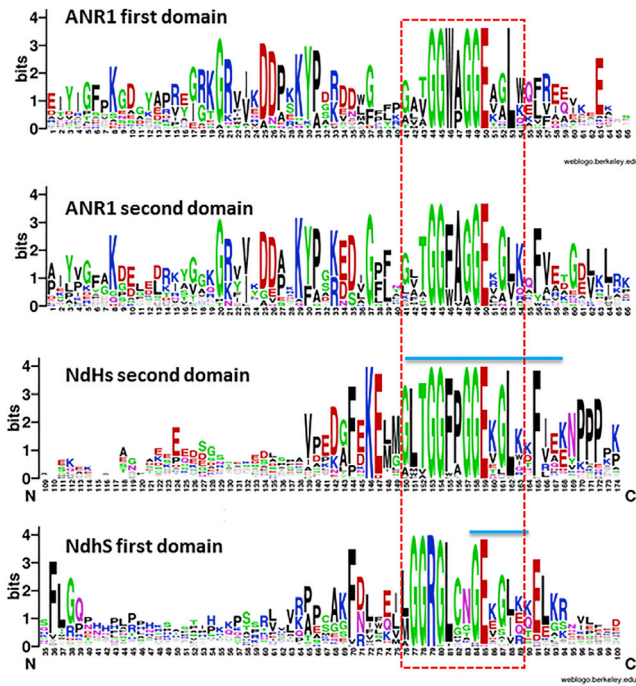


Figure 8. Sequence Logo of the Two ANR1 Domains in ANR1/ANL1 and NdhS.

The “GGE motif” is boxed. NdhS logos were generated from a sequence set dominated by land plants, which masks the high similarity between ANR1 and NdhS in Prasinophyceae. The region of high similarity to ANR1 is indicated by the blue line.

Fractionation of Thylakoid Membranes

Induction of oxic and anoxic conditions, preparation and solubilization of thylakoid membranes, and fractionation by sucrose density gradient ultracentrifugation, SDS-PAGE, and immunoblotting were performed as described by Takahashi et al. (2013).

Streptactin Affinity Purification

Thylakoid membranes (200 μ l, 160 μ g of chlorophyll) were solubilized with 0.85% n-tridecyl- β D-maltopyranoside (TDM; AppliChem, Germany) and centrifuged at 16 100 g at 4°C for 10 min. The supernatant was diluted three-fold with W1 buffer (5 mM HEPES [pH 7.5], 50 mM NaCl, 0.005% TDM) and supplemented with 170 mM NaCl before loading onto a streptactin column (Strep-trap HP, 1 ml; General Electrics, Fairfield, CT, USA) fitted to a 5-ml syringe. The column was subsequently washed with two volumes of W1 (2 \times 5 ml), then three times with 1 ml of W2 (same as W1 with 0.1% Triton X-100 added). Elution was carried out with W2 buffer containing 2.5 mM desthiobiotin (IBA, Göttingen, Germany). The column was regenerated by washing with ultrapure water and 0.5 M NaOH as described (GE Healthcare, Instructions 28-9136-30 AB).

Fluorescence Measurements

To assess the kinetics of state transitions, we used the Speedzen camera (JBeamBio, France). TAP-grown cells were placed in 96-well plates (four randomly placed technical replicates for each strain), and glucose (20 mM) and glucose oxidase (2 mg/ml) were added to induce anoxia. Fm was recorded during transition to State 2 in the dark, after which 10 μ M DCMU and 1 mM hydroxylamine were added to inhibit PSII and the light was switched on (50 μ mol photons $m^{-2} s^{-1}$) to reoxidize the PQ pool and place the cells in State 1. When the light was switched off again, the cells returned to State 2.

PETO Stimulates Cyclic Electron Flow in Anoxia

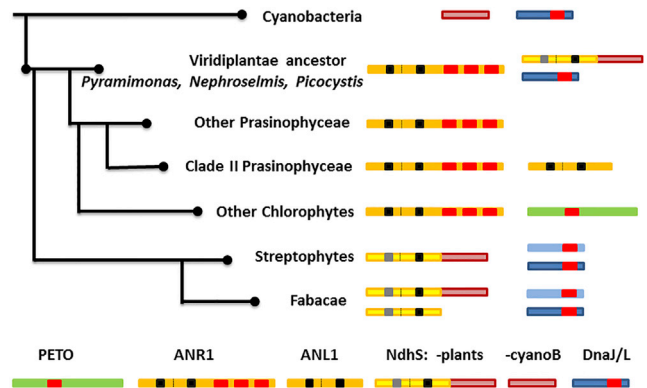


Figure 9. Evolution of PETO, ANR1, and Related Proteins.

Transmembrane helices are in red. The GGE motifs within the ANR domain are shown in black, or in gray for the first motif in NdhS to highlight its divergence.

Cyclic Electron Flow Measurements

CEF rates were determined as described previously (Takahashi et al., 2013; Clowez et al., 2015). In brief, cells harvested from exponentially growing cultures were resuspended in 20 mM HEPES (pH 7.2) and 10% Ficoll, and shaken in the dark for 30 min to place the cells in oxic conditions. A 1-ml sample was placed in the cuvette of a JTS-10 spectrophotometer (Bio-Logic, Grenoble, France), in the presence of 10 μ M DCMU. The maximal oxidation level of P700 was measured after a 100-ms saturating pulse (650 μ mol photons $m^{-2} s^{-1}$). To measure relative PSI absorption cross-section, we also recorded the initial slope of the electrochromic shift signal. Fresh samples treated with DCMU were used to measure CEF in either normoxia or anoxia, the latter being induced by addition of 20 mM glucose and 2 mg/ml glucose oxidase (Sigma-Aldrich, USA). After 5 min in the dark, pulse-induced P700 photo-oxidation was measured, after which the suspension was illuminated by red light at 135 μ mol photons $m^{-2} s^{-1}$. During illumination, steady-state and maximal P700 photo-oxidation were monitored every 10 s (the 100-ms pulse was followed by 1 s of darkness). The maximal P700 level remained constant in normoxia, while in anoxia it rose within 120 s from a few percent to >85% of the level in normoxia, indicating that acceptor side limitation was relieved. At this stage, 12 consecutive measurements of steady-state and maximal P700 oxidation were carried out every 10 s and averaged to measure CEF. Finally, the electrochromic shift measurement was carried out for anoxic samples to measure PSI antenna size in the unblocked state. To measure the CEF rate (k^{red}), we considered that at steady state $k^{red}/k^{ox} = P_{700}^{red}/(P_{700}^{ox} + P_{700}^{red})$, i.e. the fraction of the photo-oxidizable P700 that remains reduced in the light. Calculations were as described in Takahashi et al. (2013), taking into account the ECS measurements to calculate the rate of PSI charge separation (k_{ox}). CEF rates are thus expressed in electrons per second per PSI center.

Generation of Polyclonal Antibody to *Chlamydomonas* FNR

Recombinant *C. reinhardtii* FNR (Cre11.g476750 excluding the first 26 amino acids, with an N-terminal His-tag followed by an enterokinase cleavage site) was expressed in *E. coli* using a codon-adapted synthetic cDNA cloned into vector E3 (Genscript, Piscataway, NJ, USA). The protein was purified using His-tag affinity and used directly as an antigen in rabbits (Genscript, Piscataway, NJ, USA).

Analysis of Sequence Data

Protein sequences were retrieved from various sources as described in the legends of Supplemental Figures 1, 9, and 10. ClustalW alignments were manually curated in Bioedit (<http://bioedit.software.informer.com/>).

Sequence logo plots were generated using Weblogo (<http://weblogo.berkeley.edu/>). Intracellular targeting predictions used TargetP (Emanuelsson et al., 2000) at www.cbs.dtu.dk/services/TargetP and Predalgo (Tardif et al., 2012) at <https://giavap-genomes.ibpc.fr/predalgo>.

ACCESSION NUMBERS

Sequence data from this article can be found in the EMBL/GenBank data libraries under accession number GenBank: KU531882.1.

SUPPLEMENTAL INFORMATION

Supplemental Information is available at *Molecular Plant Online*.

FUNDING

This work has been financially supported by basic funding from CNRS and UPMC, the ANR-11-LABX-0011-DYNAMO, and the EU project SUNBIOPATH (Grant #245070). H.T. was supported by the Agence Nationale pour la Recherche (ANR-08-BIOE-002 Algomics) and the EU project GIAVAP (Grant #266401). J.H.L. was supported by Grant 2013M1A8A1056300 from the Korea CCS R&D Center (KCRC), Korean Ministry of Science.

AUTHOR CONTRIBUTIONS

O.V. and F.A.W. designed and supervised the study with the help of F.R. S.S. and M.S. generated the PETO amiRNA construct and J.H.L. designed the pPEARL vector. O.V. carried out sequence analysis. H.T. carried out most experiments. All authors contributed to the manuscript and approved the final version.

ACKNOWLEDGMENTS

This work has been financially supported by basic funding from CNRS and UPMC, the ANR-11-LABX-0011-DYNAMO and the EU project SUNBIOPATH (Grant #245070). HT was supported by the Agence Nationale pour la Recherche (ANR-08-BIOE-002 Algomics) and the EU project GIAVAP (Grant #266401). JHL was supported by Grant 2013M1A8A1056300 from the Korea CCS R&D Center (KCRC), Korean Ministry of Science. We thank Sunjoo Joo for help with construction of pPEARL, and Wojciech Nawrocki for critical reading of the manuscript. No conflict of interest declared.

Received: August 20, 2015

Revised: December 19, 2015

Accepted: December 21, 2015

Published: January 5, 2016

REFERENCES

Alric, J. (2010). Cyclic electron flow around photosystem I in unicellular green algae. *Photosynthesis Res.* **106**:47–56.

Alric, J. (2014). Redox and ATP control of photosynthetic cyclic electron flow in *Chlamydomonas reinhardtii*: (II) involvement of the PGR5-PGRL1 pathway under anaerobic conditions. *Biochim. Biophys. Acta* **1837**:825–834.

Bergner, S.V., Scholz, M., Trompelt, K., Barth, J., Gabelein, P., Steinbeck, J., Xue, H., Clowez, S., Fucile, G., Goldschmidt-Clermont, M., et al. (2015). STATE TRANSITION7-dependent phosphorylation is modulated by changing environmental conditions, and its absence triggers remodeling of photosynthetic protein complexes. *Plant Physiol.* **168**:615–634.

Catalanotti, C., Yang, W., Posewitz, M.C., and Grossman, A.R. (2013). Fermentation metabolism and its evolution in algae. *Front. Plant Sci.* **4**:150.

Clowez, S., Godaux, D., Cardol, P., Wollman, F.A., and Rappaport, F. (2015). The involvement of hydrogen-producing and ATP-dependent NADPH-consuming pathways in setting the redox poise in the chloroplast of *Chlamydomonas reinhardtii* in Anoxia. *J. Biol. Chem.* **290**:8666–8676.

Courteille, A., Vesa, S., Sanz-Barrio, R., Cazale, A.C., Becuwe-Linka, N., Farran, I., Havaux, M., Rey, P., and Rumeau, D. (2013). Thioredoxin m4 controls photosynthetic alternative electron pathways in *Arabidopsis*. *Plant Physiol.* **161**:508–520.

DalCorso, G., Pesaresi, P., Masiero, S., Aseeva, E., Schunemann, D., Finazzi, G., Joliot, P., Barbato, R., and Leister, D. (2008). A complex containing PGRL1 and PGR5 is involved in the switch between linear and cyclic electron flow in *Arabidopsis*. *Cell* **132**:273–285.

de Vitry, C., Finazzi, G., Baymann, F., and Kallas, T. (1999). Analysis of the nucleus-encoded and chloroplast-targeted Rieske protein by classic and site-directed mutagenesis of *Chlamydomonas*. *Plant Cell* **11**:2031–2044.

Desplats, C., Mus, F., Cuine, S., Billon, E., Cournac, L., and Peltier, G. (2009). Characterization of Nda2, a plastoquinone-reducing type II NAD(P)H dehydrogenase in *Chlamydomonas* chloroplasts. *J. Biol. Chem.* **284**:4148–4157.

Emanuelsson, O., Nielsen, H., Brunak, S., and von Heijne, G. (2000). Predicting subcellular localization of proteins based on their N-terminal amino acid sequence. *J. Mol. Biol.* **300**:1005–1016.

Finazzi, G., Rappaport, F., Furia, A., Fleischmann, M., Rochaix, J.D., Zito, F., and Forti, G. (2002). Involvement of state transitions in the switch between linear and cyclic electron flow in *Chlamydomonas reinhardtii*. *EMBO Rep.* **3**:280–285.

Fischer, N., and Rochaix, J.D. (2001). The flanking regions of Psad drive efficient gene expression in the nucleus of the green alga *Chlamydomonas reinhardtii*. *Mol. Genet. Genomics* **265**:888–894.

Fleischmann, M.M., Ravanel, S., Delosme, R., Olive, J., Zito, F., Wollman, F.A., and Rochaix, J.D. (1999). Isolation and characterization of photoautotrophic mutants of *Chlamydomonas reinhardtii* deficient in state transition. *J. Biol. Chem.* **274**:30987–30994.

Hamel, P., Olive, J., Pierre, Y., Wollman, F.A., and de Vitry, C. (2000). A new subunit of cytochrome *b₆f* complex undergoes reversible phosphorylation upon state transition. *J. Biol. Chem.* **275**:17072–17079.

Hemschemeier, A., and Happe, T. (2011). Alternative photosynthetic electron transport pathways during anaerobiosis in the green alga *Chlamydomonas reinhardtii*. *Biochim. Biophys. Acta* **1807**:919–926.

Hertle, A.P., Blunder, T., Wunder, T., Pesaresi, P., Pribil, M., Armbruster, U., and Leister, D. (2013). PGRL1 is the elusive ferredoxin-plastoquinone reductase in photosynthetic cyclic electron flow. *Mol. Cell* **49**:511–523.

Ifuku, K., Endo, T., Shikanai, T., and Aro, E.M. (2011). Structure of the chloroplast NADH dehydrogenase-like complex: nomenclature for nuclear-encoded subunits. *Plant Cell Physiol.* **52**:1560–1568.

Iwai, M., Takizawa, K., Tokutsu, R., Okamuro, A., Takahashi, Y., and Minagawa, J. (2010). Isolation of the elusive supercomplex that drives cyclic electron flow in photosynthesis. *Nature* **464**:1210–1213.

Jans, F., Mignolet, E., Houyoux, P.A., Cardol, P., Ghysels, B., Cuine, S., Cournac, L., Peltier, G., Remacle, C., and Franck, F. (2008). A type II NAD(P)H dehydrogenase mediates light-independent plastoquinone reduction in the chloroplast of *Chlamydomonas*. *Proc. Natl. Acad. Sci. USA* **105**:20546–20551.

Johnson, G.N. (2011). Physiology of PSI cyclic electron transport in higher plants. *Biochim. Biophys. Acta* **1807**:384–389.

Johnson, X., Steinbeck, J., Dent, R.M., Takahashi, H., Richaud, P., Ozawa, S., Houille-Vernes, L., Petroustos, D., Rappaport, F., Grossman, A.R., et al. (2014). Proton gradient regulation 5-mediated cyclic electron flow under ATP- or redox-limited conditions: a study of DeltaATPase pgr5 and Deltarbcl pgr5 mutants in the green alga *Chlamydomonas reinhardtii*. *Plant Physiol.* **165**:438–452.

- Joliot, P., and Johnson, G.N. (2011). Regulation of cyclic and linear electron flow in higher plants. *Proc. Natl. Acad. Sci. USA* **108**:13317–13322.
- Lemaire, C., Girard-Bascou, J., Wollman, F.-A., and Bennoun, P. (1986). Studies on the cytochrome *b₆f* complex. I. Characterization of the complex subunits in *Chlamydomonas reinhardtii*. *Biochim. Biophys. Acta* **851**:229–238.
- Lemieux, C., Otis, C., and Turmel, M. (2014). Six newly sequenced chloroplast genomes from prasinophyte green algae provide insights into the relationships among prasinophyte lineages and the diversity of streamlined genome architecture in picoplanktonic species. *BMC Genomics* **15**:857.
- Majeran, W., Olive, J., Drapier, D., Vallon, O., and Wollman, F.A. (2001). The light sensitivity of ATP synthase mutants of *Chlamydomonas reinhardtii*. *Plant Physiol.* **126**:421–433.
- Miyake, C. (2010). Alternative electron flows (water-water cycle and cyclic electron flow around PSI) in photosynthesis: molecular mechanisms and physiological functions. *Plant Cell. Physiol.* **51**:1951–1963.
- Molnar, A., Bassett, A., Thuenemann, E., Schwach, F., Karkare, S., Ossowski, S., Weigel, D., and Baulcombe, D. (2009). Highly specific gene silencing by artificial microRNAs in the unicellular alga *Chlamydomonas reinhardtii*. *Plant J.* **58**:165–174.
- Munekage, Y., Hojo, M., Meurer, J., Endo, T., Tasaka, M., and Shikanai, T. (2002). PGR5 is involved in cyclic electron flow around photosystem I and is essential for photoprotection in *Arabidopsis*. *Cell* **110**:361–371.
- Nawrocki, W.J., Tourasse, N.J., Taly, A., Rappaport, F., and Wollman, F.A. (2015). The plastid terminal oxidase: its elusive function points to multiple contributions to plastid physiology. *Annu. Rev. Plant Biol.* **66**:49–74.
- Ossowski, S., Schwab, R., and Weigel, D. (2008). Gene silencing in plants using artificial microRNAs and other small RNAs. *Plant J.* **53**:674–690.
- Petroutsos, D., Busch, A., Janssen, I., Trompelt, K., Bergner, S.V., Weinl, S., Holtkamp, M., Karst, U., Kudla, J., and Hippler, M. (2011). The chloroplast calcium sensor CAS is required for photoacclimation in *Chlamydomonas reinhardtii*. *Plant Cell* **23**:2950–2963.
- Rochaix, J.D. (2014). Regulation and dynamics of the light-harvesting system. *Annu. Rev. Plant Biol.* **65**:287–309.
- Schmollinger, S., Strenkert, D., and Schroda, M. (2010). An inducible artificial microRNA system for *Chlamydomonas reinhardtii* confirms a key role for heat shock factor 1 in regulating thermotolerance. *Curr. Genet.* **56**:383–389.
- Schröda, M., Beck, C.F., and Vallon, O. (2002). Sequence elements within an HSP70 promoter counteract transcriptional transgene silencing in *Chlamydomonas*. *Plant J.* **31**:445–455.
- Shikanai, T. (2007). Cyclic electron transport around photosystem I: genetic approaches. *Annu. Rev. Plant Biol.* **58**:199–217.
- Shikanai, T. (2014). Central role of cyclic electron transport around photosystem I in the regulation of photosynthesis. *Curr. Opin. Biotechnol.* **26**:25–30.
- Shikanai, T., Endo, T., Hashimoto, T., Yamada, Y., Asada, K., and Yokota, A. (1998). Directed disruption of the tobacco *ndhB* gene impairs cyclic electron flow around photosystem I. *Proc. Natl. Acad. Sci. USA* **95**:9705–9709.
- Sizova, I., Fuhrmann, M., and Hegemann, P. (2001). A *Streptomyces rimosus* aphVIII gene coding for a new type phosphotransferase provides stable antibiotic resistance to *Chlamydomonas reinhardtii*. *Gene* **277**:221–229.
- Stroebel, D., Choquet, Y., Popot, J.L., and Picot, D. (2003). An atypical haem in the cytochrome b(6)f complex. *Nature* **426**:413–418.
- Takahashi, H., Clowez, S., Wollman, F.A., Vallon, O., and Rappaport, F. (2013). Cyclic electron flow is redox-controlled but independent of state transition. *Nat. Commun.* **4**:1954–1961.
- Tardif, M., Atteia, A., Specht, M., Cogne, G., Rolland, N., Brugiere, S., Hippler, M., Ferro, M., Bruley, C., Peltier, G., et al. (2012). PredAlgo: a new subcellular localization prediction tool dedicated to green algae. *Mol. Biol. Evol.* **29**:3625–3639.
- Terashima, M., Specht, M., Naumann, B., and Hippler, M. (2010). Characterizing the anaerobic response of *Chlamydomonas reinhardtii* by quantitative proteomics. *Mol. Cell. Proteomics* **9**:1514–1532.
- Terashima, M., Petroutsos, D., Hudig, M., Tolstygina, I., Trompelt, K., Gabelein, P., Fufezan, C., Kudla, J., Weinl, S., Finazzi, G., et al. (2012). Calcium-dependent regulation of cyclic photosynthetic electron transfer by a CAS, ANR1, and PGRL1 complex. *Proc. Natl. Acad. Sci. USA* **109**:17717–17722.
- Tolleter, D., Ghysels, B., Alric, J., Petroutsos, D., Tolstygina, I., Krawietz, D., Happe, T., Auroy, P., Adriano, J.M., Beyly, A., et al. (2011). Control of hydrogen photoproduction by the proton gradient generated by cyclic electron flow in *Chlamydomonas reinhardtii*. *Plant Cell* **23**:2619–2630.
- Vallon, O., Bulte, L., Dainese, P., Olive, J., Bassi, R., and Wollman, F.A. (1991). Lateral redistribution of cytochrome b6/f complexes along thylakoid membranes upon state transitions. *Proc. Natl. Acad. Sci. USA* **88**:8262–8266.
- Wang, C., Yamamoto, H., and Shikanai, T. (2015). Role of cyclic electron transport around photosystem I in regulating proton motive force. *Biochim. Biophys. Acta* **1847**:931–938.
- Wei, L., Derrien, B., Gautier, A., Houille-Vernes, L., Boulouis, A., Saint-Marcoux, D., Malnoe, A., Rappaport, F., de Vitry, C., Vallon, O., et al. (2014). Nitric oxide-triggered remodeling of chloroplast bioenergetics and thylakoid proteins upon nitrogen starvation in *Chlamydomonas reinhardtii*. *Plant Cell* **26**:353–372.
- Wollman, F.A. (2001). State transitions reveal the dynamics and flexibility of the photosynthetic apparatus. *EMBO J.* **20**:3623–3630.
- Wollman, F.A., and Delepelaire, P. (1984). Correlation between changes in light energy distribution and changes in thylakoid membrane polypeptide phosphorylation in *Chlamydomonas reinhardtii*. *J. Cell. Biol.* **98**:1–7.
- Yamamoto, H., and Shikanai, T. (2013). In planta mutagenesis of Src homology 3 domain-like fold of NdhS, a ferredoxin-binding subunit of the chloroplast NADH dehydrogenase-like complex in *Arabidopsis*: a conserved Arg-193 plays a critical role in ferredoxin binding. *J. Biol. Chem.* **288**:36328–36337.
- Yamamoto, H., Peng, L., Fukao, Y., and Shikanai, T. (2011). An Src homology 3 domain-like fold protein forms a ferredoxin binding site for the chloroplast NADH dehydrogenase-like complex in *Arabidopsis*. *Plant Cell* **23**:1480–1493.
- Zito, F., Finazzi, G., Delosme, R., Nitschke, W., Picot, D., and Wollman, F.A. (1999). The Qo site of cytochrome *b₆f* complexes controls the activation of the LHClI kinase. *EMBO J.* **18**:2961–2969.